

HST/STIS Lyman- α observations of the quiet M dwarf GJ 436

Predictions for the exospheric transit signature of the hot neptune GJ 436b[★]

D. Ehrenreich¹, A. Lecavelier des Etangs² & X. Delfosse¹

¹ Institut de planétologie et d'astrophysique de Grenoble (IPAG), Université Joseph Fourier-Grenoble 1, CNRS (UMR 5274), BP 53 38041 Grenoble CEDEX 9, France, e-mail: david.ehrenreich@obs.ujf-grenoble.fr

² Institut d'astrophysique de Paris, Université Pierre et Marie Curie, CNRS (UMR 7095), 98 bis boulevard Arago, 75014 Paris, France

ABSTRACT

Lyman- α ($Ly\alpha$) emission of neutral hydrogen ($\lambda 1215.67$ Å) is the main contributor to the ultraviolet flux of low-mass stars such as M dwarfs. It is also the main light source used in studies of the evaporating upper atmospheres of transiting extrasolar planets with ultraviolet transmission spectroscopy. However, there are very few observations of the $Ly\alpha$ emissions of quiet M dwarfs, and none exist for those hosting exoplanets. Here, we present $Ly\alpha$ observations of the hot-neptune host star GJ 436 with the *Hubble Space Telescope* Imaging Spectrograph (*HST/STIS*). We detect bright emission in the first resolved and high quality spectrum of a quiet M dwarf at $Ly\alpha$. Using an energy diagram for exoplanets and an N -body particle simulation, this detection enables the possible exospheric signature of the hot neptune to be estimated as a $\sim 11\%$ absorption in the $Ly\alpha$ stellar emission, for a typical mass-loss rate of 10^{10} g s⁻¹. The atmosphere of the planet GJ 436b is found to be stable to evaporation, and should be readily observable with *HST*. We also derive a correlation between X-ray and $Ly\alpha$ emissions for M dwarfs. This correlation will be useful for predicting the evaporation signatures of planets transiting other quiet M dwarfs.

Key words. ultraviolet: planetary systems – planets and satellites: individual: GJ 436b – planets and satellites: atmospheres – stars: low-mass – stars: activity – techniques: spectroscopic

1. Introduction

Planetary transits provide golden opportunities to probe the atmospheres of extrasolar planets. The atmospheric signals detected by this method in the visible (e.g., Charbonneau et al. 2002) are usually tenuous, while the infrared detections of atmospheric signatures remain disputed (e.g., Gibson, Pont & Aigrain 2010). In the ultraviolet (UV), planetary transits of the hot giant planet HD 209458b are detected from conspicuous spectroscopic signatures, which are seen as absorption in the emission lines originating from the stellar chromosphere and transition region between the chromosphere and the corona (see Ehrenreich 2010 for a review). The strongest signature is a $(15 \pm 4)\%$ absorption in the resolved stellar Lyman- α ($Ly\alpha$) emission line of neutral atomic hydrogen (H I) detected in medium-resolution spectra taken with the Space Telescope Imaging Spectrograph (STIS) on the *Hubble Space Telescope* (*HST*) (Vidal-Madjar et al. 2003; see also Ehrenreich et al. 2008). Linsky et al. (2010) present new observations with the Cosmic Origins Spectrograph (COS) on *HST*. They report a $(7.8 \pm 1.3)\%$ absorption in the C II line, confirming the previous result of Vidal-Madjar et al. (2004).

These distinctive UV signatures, compared to those for the visible transit of the whole planet (1.6%; Charbonneau et al. 2000; Henry et al. 2000), require the presence of an extended H I upper atmosphere, or exosphere, to the planet. This envelope must be evaporating because (i) it must fill the planetary Roche lobe to account for the size of the absorption, and (ii) the H I atoms must be accelerated by the stellar radiation pressure be-

yond the escape velocity of the planet to account for the absorption in the wings of the $Ly\alpha$ line (Vidal-Madjar et al. 2003). The presence of elements heavier than hydrogen (C, O, Si) at high altitudes requires an hydrodynamic escape (or blow-off) of the upper atmosphere, with the flow of escaping H I carrying heavier species up to the Roche limit (Vidal-Madjar et al. 2004; Linsky et al. 2010), where they are swept away by radiation pressure (Lecavelier des Etangs, Vidal-Madjar & Désert 2008).

New cases of atmospheric escape have been recently reported for two hot jupiters. Lecavelier des Etangs et al. (2010) used *HST/ACS* to detect the H I exosphere of HD 189733b at $Ly\alpha$. Fossati et al. (2010) observed the highly irradiated planet host star WASP-12 with *HST/COS*. They interpret the tentative detection of extra absorption in the metal lines of the star WASP-12 during the transit as signs of mass loss. Thus, atmospheric evaporation could be a common phenomenon among close-in planets.

These results have inspired a comprehensive modelling effort (e.g., García-Muñoz 2007) suggesting that the upper atmospheres of close-in giant planets must be heated by the stellar X-rays, and both extreme and far UV (Cecchi-Pestellini et al. 2009) to about 10 000 K. This temperature has been inferred in the thermosphere of HD 209458b from the detection of excited hydrogen atoms (Ballester, Sing & Herbert 2007). The typical atmospheric mass-loss rate \dot{m} derived from models is between 10^{10} and 10^{11} g s⁻¹. In this case, evaporation should not severely impact the stability of giant planets' atmospheres. On the other hand, it might be more important for lower-mass planets such as hot neptunes and super-earths, if their mass-loss rates are of the same order as for more massive planets.

In this article, we evaluate whether mass loss from a hot neptune such as GJ 436b could be detected with current instru-

Send offprint requests to: D. Ehrenreich

[★] Based on observations made with the Space Telescope Imaging Spectrograph on board the *Hubble Space Telescope* (Cycle 17 program GO/DD 11817)

Table 1. Properties of GJ 436 and its planet

Parameter	Value	Ref.
The planet		
Mass M_p (M_{\oplus})	23.17 ± 0.79	(1)
Radius R_p (R_{\oplus})	$4.22^{+0.09}_{-0.10}$	(1)
Mean density ρ_p (g cm^{-3})	$1.69^{+0.14}_{-0.12}$	(1)
Gravity g_p (m s^{-2})	12.8 ± 0.8	(1)
Semi-major axis a_p (AU)	0.02872 ± 0.00027	(1)
Brightness temperature T_B (K)	717 ± 35	(3)
The star		
Distance d_{\star} (pc)	10.23 ± 0.24	(4)
X/EUV luminosity		
$\log(L_{X/EUV} [\text{erg s}^{-1}])$	$26.85^{+0.65}_{-0.89}$	(2)

Notes. (1) Torres 2007; (2) H \ddot{u} nsch et al. 1999, Sanz-Forcada et al. 2010, Poppenhaefer et al. 2010; (3) Demory et al. 2007; (4) *Hipparcos* catalogue, Perryman et al. 1997.

mentation, and what its UV transit signature could be. GJ 436b is the first transiting Neptune-mass planet discovered (Butler et al. 2004). It orbits a close-by (10.2 pc) M2.5v dwarf with $V = 10.68$, and triggered unprecedented interest when Gillon et al. (2007a) detected a photometric transit of the planet, inferring a true mass of $23.17 M_{\oplus}$ and a radius of $4.22 R_{\oplus}$, which are similar to those of either Uranus or Neptune. (The planet properties, taken from Torres (2007), are summarized in Table 1 along with some stellar parameters.) However, GJ 436b differs significantly from the Solar System ice giants because of its moderately eccentric orbit with a semi-major axis of 0.029 astronomical unit (AU). At this distance from its 0.026- L_{\odot} parent star, the planet indeed receives $\sim 30\,000$ times more flux than Neptune receives from the Sun, and has a blackbody brightness temperature of $T_B = 717 \pm 35$ K (Demory et al. 2007). Using the *Spitzer Space Telescope*, Gillon et al. (2007b) inferred a planet mean density of $\sim 1.7 \text{ g cm}^{-3}$, too weak to be that of a body composed exclusively of water ice, so that GJ 436b must possess a hydrogen/helium envelope that would account for $\sim 10\%$ to 20% of the planet’s mass (Fortney et al. 2007; Figueira et al. 2009). The detection of this envelope with transmission spectroscopy could validate the internal structure models predicting its presence.

To assess this possibility, it is necessary to derived both the stellar Ly α emission line profile and brightness. We present in Sect. 2 the observations that allowed us to calculate the stellar emission as seen from Earth. We had to correct for the interstellar medium (ISM) absorption before estimating the intrinsic stellar Ly α brightness: this analysis is presented in Sect. 3. In Sect. 4, we estimate a range of plausible mass-loss rates in GJ 436b’s upper atmosphere. This range serves as an input to an atmospheric escape model used to estimate the transit signature of the evaporating hydrogen envelope of the planet in the UV (Sect. 5). To our knowledge, these observations are the first resolved accurate measurement of a quiet M dwarf’s Ly α emission. Hence, we discuss in Sect. 6 how they compare to archival Ly α observations of active M dwarfs.

2. Observations and data reduction

We obtained *HST* time (GO/DD#11817) to precisely estimate the Ly α emission of the M dwarf GJ 436. The data were recorded on 2010 January 6 with the STIS instrument (Woodgate et al. 1997). The observation consists of one 1762-s exposure on the Far Ultraviolet Multi-Anode Microchannel Array detector (FUV-MAMA). The STIS/FUV-MAMA is a solar-blind cesium iodide (CsI) detector with a $25'' \times 25''$ field of view

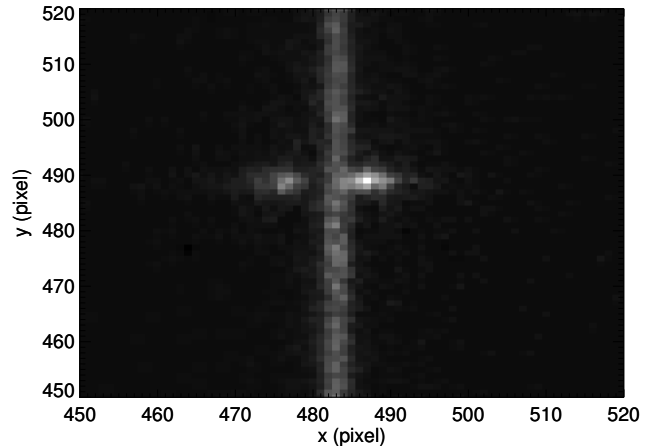


Fig. 1. Two-dimensional spectral image of GJ 436. The light is dispersed along the x-axis (roughly). The stellar Ly α emission is seen on both sides of the geocoronal emission, which impacts the detector across the whole y-axis.

($\sim 0'.025 \text{ pixel}^{-1}$), operating from 1 150 to 1 700 \AA . The light was diffracted using the long slit of size $52'' \times 0'.1$ and the first-order grating G140M. This grating was tilted to ensure a central wavelength of 1 222 \AA . In this configuration, our data have a spectral coverage of 1 194–1 249 \AA with a medium resolution of $\sim 10\,000$ (30 km s^{-1}) and a throughput of between $\sim 1.2\%$ and 2% (see Proffitt et al. 2010). The data were recorded in time-tag mode, and treated with the version 2.27 of CALSTIS, the STIS data pipeline. CALSTIS performs all the standard data reduction tasks (such as bias and dark subtraction, flat fielding, and wavelength and flux calibrations; see Dressel et al. 2007 for more details). For spectroscopy, the pipeline end-products for a single exposure are the two-dimensional spectral image and the one-dimensional spectrum.

Figure 1 shows the geometrically rectified, wavelength-, and flux-calibrated 2-D spectral image (X2D). The spectral dispersion is along the x-axis. In this image, the stellar Ly α emission appears on both sides of the prominent geocoronal emission, which is imaged across the whole detector y-axis. This terrestrial air glow seriously degrades the quality of spectroscopic observations at Ly α ; however its rather narrow extent along the dispersion (x-)axis and its large spatial extent (y-axis) enable us to perform an efficient correction. This task is handled by the pipeline subroutine called BACKCORR, which performs the 1-D spectral background subtraction. The background is determined along a five-pixel-wide region located ± 300 pixels away from the centre of the spectral extraction region. The 1-D extracted background is then fitted by a n -th degree polynomial, which replaces the background *except* in the regions surrounding the Ly α line (Dressel et al. 2007). The resulting calibrated 1-D spectrum of GJ 436 (X1D) is shown in Fig. 2.

3. Lyman- α emission of GJ 436

3.1. Observed flux at Earth

Figure 3 shows a zoomed region of the recorded spectrum around the Ly α line. The error bar for each spectral bin is estimated by CALSTIS, which basically propagates the statistical noise $\sqrt{(Ng)/g}$ in each pixel of the raw data, where N is the

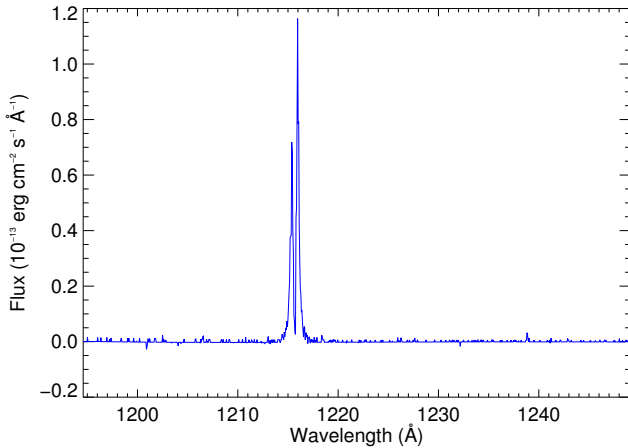


Fig. 2. The reduced and calibrated STIS/G140M spectrum of GJ 436 in January 2010.

number of data events (counts) and g is the gain (equal to 1 photon count⁻¹ for MAMA observations).

The total flux of the line seen by *HST*, integrated from 1214.40 to 1215.58 Å and from 1215.75 to 1217.00 Å in order to avoid any residuals from the air glow subtraction at the centre of the line, is $(5.490 \pm 0.184) \times 10^{-14}$ erg s⁻¹ cm⁻². We note that, as seen from the Earth, the $\text{Ly}\alpha$ flux of GJ 436 is higher than that of HD 209458b: the stellar emission from the latter star is also reproduced in Fig. 3 for comparison.

The observed shape of the line is a characteristic double peak resulting from the addition of several profiles, as shown in Fig. 4. As for the Sun (Woods et al. 2005), the core of the intrinsic stellar $\text{Ly}\alpha$ line is an emission feature originating in the transition region, where the temperature increases quickly between the chromosphere and the corona. The wings of the $\text{Ly}\alpha$ line originate in a deeper chromospheric region. The emission can be either single-peaked or double-peaked, with a central dip due to the high opacity of the abundant hydrogen atoms. As seen from the Solar System, the central part of the line is strongly absorbed by the ISM from 1215.58 to 1215.75 Å. The ISM absorption can indeed be Doppler-shifted relative to the line centre by several kilometers per second. The ISM absorption is the combination of absorption by neutral hydrogen (H I) and deuterium (D I). Deuterium produces narrow absorption at 1215.3 Å, which is blue-shifted by ~ 0.3 Å from the H I absorption line. The observed $\text{Ly}\alpha$ profile is therefore caused by the stellar emission line being absorbed by the ISM and subsequently convolved with the instrumental line spread function (Fig. 4).

3.2. Reconstructed stellar intrinsic emission

To model the hydrogen atom dynamics under the stellar $\text{Ly}\alpha$ radiation pressure, we need to estimate the stellar emission line as seen by hydrogen atoms escaping from the planet. To calculate the resulting $\text{Ly}\alpha$ transit light curve, we also need to estimate the absorption by the escaping atoms over the stellar profile as seen from the Earth (Sect. 5). To produce these two line profiles, we fitted the observed $\text{Ly}\alpha$ profile with a stellar emission line and an ISM absorption model, following the method proposed by Wood et al. (2005). In the following, we assume a D/H ratio of 1.5×10^{-5} . There is widespread consensus (e.g., Ferlet et al.

2000; Hébrard & Moos 2003; Linsky et al. 2006) that this value of the D/H ratio is constant within the Local Bubble (< 100 pc; see Wood et al. 2005 and references therein).

The ISM column density value is chosen within the range considered by Wood et al. (2005), $17.6 < \log N(\text{H I}) < 18.2$. The value is adjusted to 10^{18} cm⁻² using the D I line at 1215.25 Å. This agrees with the ISM column density of $\log N(\text{H I}) = 17.82$ measured by Wood et al. (2005) toward the star HD 4345, in a similar direction (11.1° from GJ 436) and at a distance of 21.7 pc. A column density $\log N(\text{H I}) \gg 18$ would be unrealistic for a target as close as GJ 436 (10.2 pc) and yield a stronger D I absorption than observed. (The presence of this feature can be guessed in the blue part of the observed H I $\text{Ly}\alpha$ emission in Fig. 3.) In any case, the fit to the observed $\text{Ly}\alpha$ profile does not depend much on the assumed ISM column density between $N(\text{H I}) \sim 10^{17}$ and 10^{18} cm⁻² because at these column densities, the H I absorption line is saturated. The result is more dependent on the assumed profile of the wings extrapolated to the core of the emission line.

As pointed out by Wood et al. (2005), the reconstruction of the intrinsic $\text{Ly}\alpha$ emission of a star can be affected by absorption from both the heliosphere and the astrosphere, which we did not model for GJ 436. Owing to the moderate resolution of the present observations and our lack of knowledge about the ISM absorption, from either D I or heavier elements (Fe II or Mg II), this absorption remain unconstrained. However, GJ 436 is located 87.7° from the upwind direction of the ISM flow seen by the Sun, hence based on Fig. 13 in Wood et al. (2005) it is unlikely that heliospheric absorption is detectable. No extra H I absorption is required besides the ISM component to achieve a good fit of the $\text{Ly}\alpha$ line. In particular, we did not consider an astrospheric absorption component. Wood et al. (2005) found that this absorption was necessary in some case to obtain satisfactory fits to the $\text{Ly}\alpha$ lines. This does not seem to be the case for GJ 436 given the current data resolution.

We performed the model fitting using several intrinsic line profiles, including a single-peak Gaussian and a double-peaked line modelled by a double Gaussian. We found that the double-peaked Gaussian reproduces far more accurately the observed wings in the line profile. The model intrinsic profile is composed of two Gaussians with the same full width at half maximum ($\text{FWHM} = \Delta\lambda$) and line centres separated by the same value, $\Delta\lambda$, which is taken as a free parameter. The line total flux is the second free parameter. The ISM and the stellar radial velocities are also free parameters. The model is convolved with the G140M instrumental line spread function, and compared to the observations. We found a satisfactory fit with $\Delta\lambda = 0.41$ Å, an ISM radial velocity of -4 km s⁻¹ in the stellar reference frame, and a stellar radial velocity corresponding to a Doppler shift of 0.003 Å (~ 0.7 km s⁻¹). The resulting χ^2 is 34.5 for 39 degrees of freedom (see the data and fit in Fig. 4).

The total flux in the reconstructed $\text{Ly}\alpha$ line is $(2.7 \pm 0.7) \times 10^{-13}$ erg s⁻¹ cm⁻². The error bars were estimated by exploring the parameter space for the fit to the observed H I line wings, and considering possible single-peaked profiles or the possibility of two narrow peaks with a deep self-absorption in the central part of the emission line. These last two cases produce extreme $\text{Ly}\alpha$ emission profiles within the ISM absorbed wavelength range; the resulting error bars should be considered as conservative.

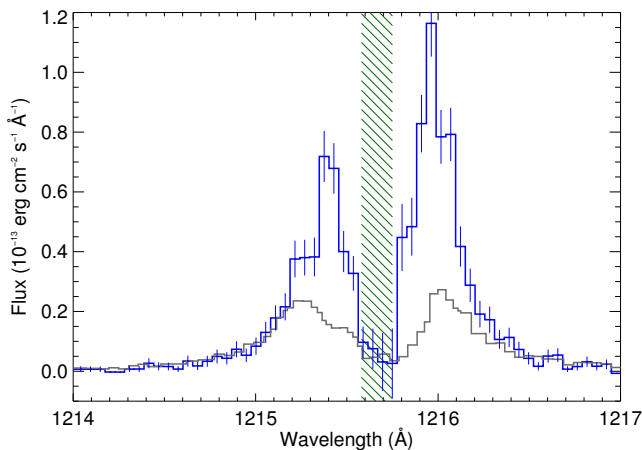


Fig. 3. Zoom on the $\text{Ly}\alpha$ line of GJ 436 measured with STIS/G140M with error bars from the STIS pipeline (blue curve). The STIS spectrum of HD 209458 obtained by Vidal-Madjar et al. (2003) is shown for comparison (grey curve). As seen from Earth, the nearby M dwarf clearly shows a more intense stellar emission and a narrower ISM absorption. The location of the air glow (subtracted here) is indicated by green hatches.

4. Mass-loss rate of GJ 436b

The mass-loss rate \dot{m} of GJ 436b is a free parameter in our modelling of the evaporation signature described in the next section. Nevertheless, estimating its value is useful to constraining all the parameter space. To achieve this, we use the method presented by Lecavelier des Etangs (2007), which consists of locating the planet in an “energy diagram”. The energy diagram of exoplanets measures the whole gravitational potential energy of a planet, as a function of high-energy irradiations it receives. This diagram was updated by Davis & Wheatley (2009), and is being completed with a larger sample of transiting planets (Ehrenreich & Désert 2011), including GJ 436.

The resulting diagram is presented in Fig. 5. For GJ 436, we calculate, following Lecavelier des Etangs (2007), the potential energy per mass unit of the planet

$$\frac{dE'_p}{dm} = -GM_p/R_p + \delta_{\text{tides}} = -2.05 \times 10^{12} \text{ erg g}^{-1}, \quad (1)$$

where G is the gravitational constant and δ_{tides} is the modification of the planet gravitational potential by the stellar tides (see Appendix B of Lecavelier des Etangs 2007).

The energy received by unit of time by GJ 436b can be expressed as

$$\frac{dE_{\text{X/EUV}}}{dt} = \frac{\eta}{4} R_p^2 a_p^{-2} L_{\text{X/EUV}} = 2.19 \times 10^{22} \eta \text{ erg s}^{-1}. \quad (2)$$

The ‘X/EUV’ in $L_{\text{X/EUV}}$ means that the luminosity should be integrated from $\sim 1 \text{ \AA}$ to 912 \AA , following Cecchi-Pestellini et al. (2009).¹ However, observations do not usually cover a sufficiently wide bandpass to yield a precise value of $L_{\text{X/EUV}}$. The

¹ In this paper, we use the following conventions for naming spectral regions: X-rays (X) in 1–10 \AA , soft X-rays (XUV) in 10–30 \AA , extreme ultraviolet (EUV) in 30–912 \AA , and far ultraviolet (FUV) in 912–1216 \AA .

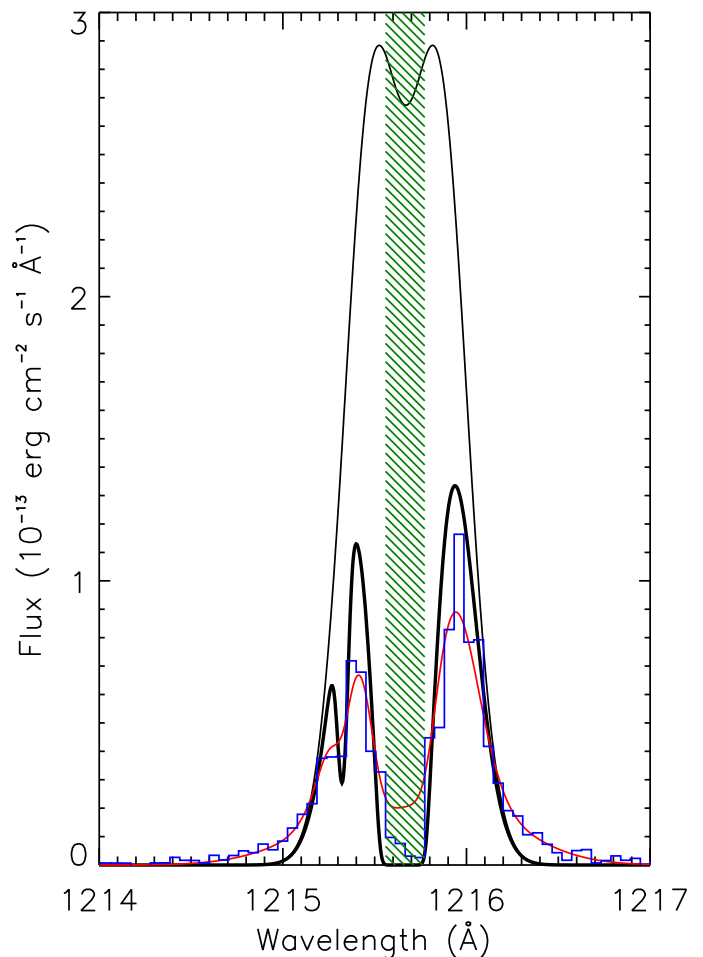


Fig. 4. Plot of the theoretical profile of GJ 436’s $\text{Ly}\alpha$ line. The black thin line shows the intrinsic stellar emission line as seen by hydrogen atoms escaping the planetary atmosphere. The black thick line shows the resulting profile after absorption by the ISM hydrogen and deuterium. The line profile convolved with the *HST* G140M instrumental line spread function (red line) is compared to the observations (blue histogram), yielding a good fit with a χ^2 of 34.5 for 39 degrees of freedom. The location of the (subtracted) air glow is indicated by green hatches.

Rosat luminosity (Hünsch et al. 1999) given in Table 1 is calculated from 0.1 to 2.4 keV, i.e., from 5 to 124 \AA . It is, therefore, a lower limit to the actual X/EUV luminosity.

The factor η is the heating efficiency in the exoplanet thermosphere. Lecavelier des Etangs (2007) considered the extreme case of $\eta = 1$ where all the stellar flux is used to escape the atmosphere. Considering (without quantifying) energetic losses due to thermal emission by atmospheric hydrogen, Tian et al. (2005) modelled the atmospheric escape process of the hot Jupiter HD 209458b by assuming that $\eta = 0.15$. This value was initially chosen by Watson, Donahue & Walker (1981) in their pioneering study of Earth’s atmospheric escape. In the following, we consider both of these values of η .

The resulting mass-loss rate is thus

$$\dot{m} = -\eta \frac{dE_{\text{X/EUV}}}{dE'_p}. \quad (3)$$

For $\eta = 1$ and 0.15, we find that $\dot{m} = 1.07 \times 10^{10}$ and $1.60 \times 10^9 \text{ g s}^{-1}$, respectively. These values are close to the

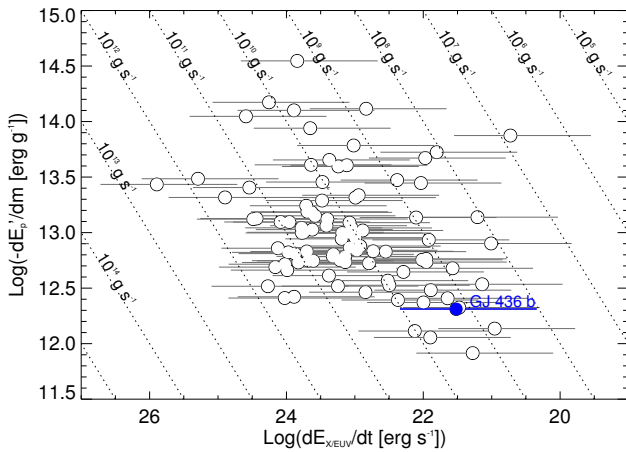


Fig. 5. Energy diagram for 100 transiting exoplanets, updated from Lecavelier des Etangs 2007. The energy needed to escape a unit of mass of the planet atmosphere is plotted versus the X/EUV flux. The dotted lines indicate constant mass-loss rates. The blue dot indicates the location of GJ 436b, calculated here assuming an heating efficiency of $\eta = 0.15$. The horizontal error bars represent variations in η of between 0.01 and 1.

canonical escape rate predicted by several evaporation models (e.g., Yelle 2004, 2006; Lecavelier des Etangs et al. 2004; García-Muñoz 2007; Murray-Clay, Chiang & Murray 2009).

5. Observable signature of the evaporating atmosphere

To calculate a theoretical H I transit light curve for various atmospheric escape rates, we modelled the atmospheric gas escaping GJ 436b with a numerical simulation including the dynamics of the hydrogen atoms. In this N -body simulation, hydrogen atoms are released from GJ 436b's upper atmosphere as particles with a random initial velocity corresponding to a 10 000-K exobase. This temperature corresponds to the temperature expected in the upper atmospheres of hot Jupiters (e.g., Lecavelier des Etangs et al. 2004; Stone & Proga 2009) and was inferred from observations (Ballester, Sing & Herbert 2007; Vidal-Madjar et al. 2011). In any case, our results do not depend on this assumption because atoms are rapidly accelerated by the radiation pressure to velocities several times higher than their initial velocities. In this model, the gravity of both the star and the planet are taken into account. The radiation pressure from the stellar Ly α emission line is calculated as a function of the radial velocity of the atoms. The self-extinction within the cloud is also taken into account. The hydrogen atoms are supposed to be ionized by the stellar EUV flux ($< 912 \text{ \AA}$). In the simulation, their lifetime is calculated as a function of the ionizing EUV flux which is taken to be equal to the solar value. The only free parameter is the atomic hydrogen escape rate, expressed in grams per second. The dynamical model provides a steady state distribution of positions and velocities of escaping hydrogen atoms in the cloud surrounding GJ 436b. From this information, we calculated the corresponding absorption over the stellar line (Fig. 6) and the corresponding transit light curve of the total Ly α line (Fig. 7). We found that escape rates of $\sim 10^9$ to 10^{10} g s^{-1} can produce absorptions of between $\sim 3\%$ and 11% in the Ly α transit light curve when integrating over the whole line. Absorption depths

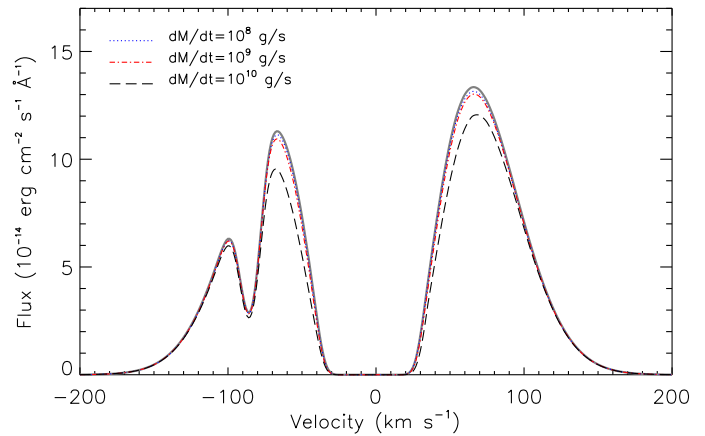


Fig. 6. The GJ 436 Ly α spectrum during the transit of GJ 436b. The star spectrum before or after the transit is shown by a thick grey line. The spectrum resulting from the absorption by the planetary exosphere during the transit is shown for various escape rates. The blue dotted, the red dot-dashed, and black long-dashed lines show the resulting spectrum when the escape rate is 10^8 , 10^9 , and 10^{10} g s^{-1} , respectively. With this last escape rate, the blue side of the line is absorbed by about 17%, resulting in a decrease of about 11% in the total Lyman- α flux.

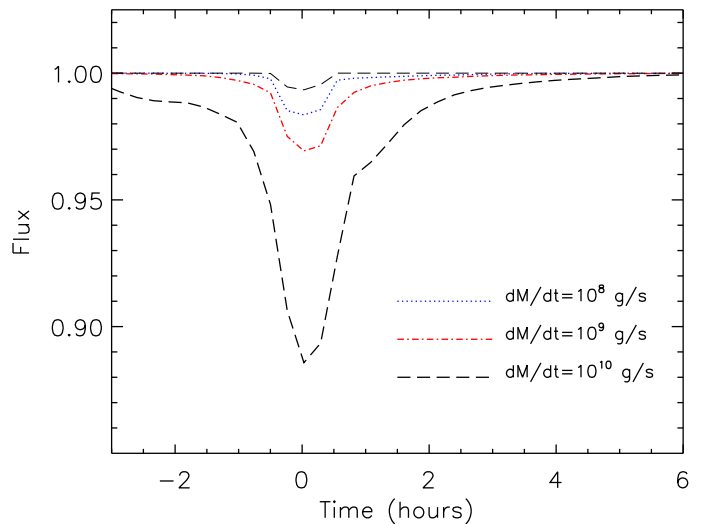


Fig. 7. Plot of the theoretical light curve of the total Ly α flux for various escape rates \dot{m} : 10^8 g s^{-1} (blue dotted line), 10^9 g s^{-1} (red dot-dashed line), and 10^{10} g s^{-1} (black dashed line). The thin long-dashed line shows the light curve for the planet without additional absorption by the planetary atmosphere.

this large could be promptly detected with *HST* Ly α observations.

This contrasts with the atmospheric signatures expected in the infrared. The atmospheric scale height of this planet is $H = k_B T_B / (\mu g_p) \approx 232 \text{ km}$, where $\mu = 2 \text{ g mol}^{-1}$ is the molar mass of a H $_2$ atmosphere and g_p is the surface gravity of the planet. We can expect atmospheric transit signatures at the level of $\sim 2(\Delta F/F)(H/R_p)$ (Winn 2010), where $\Delta F/F \approx (R_p/R_\star)^2 \approx 0.7\%$ is the transit occultation. This yields a typical extra absorption value of $\sim 10^{-4}$ for one atmospheric scale height. This value is consistent with the upper limits on the atmospheric absorp-

tion of GJ 436b set by Pont et al. (2009), who have covered two near-infrared transits of the planet with the NICMOS camera on *HST* using a grism to sample the 1.1–1.9 μm band. These authors report observing a flat transmission spectrum at the level of $\sim 10^{-4}$, and in particular no significant signal in the 1.4- μm water band (see also Gibson, Pont & Aigrain 2010).

Using eclipses of the planet by the star observed by *Spitzer*, Stevenson et al. (2010) obtained planet-to-star flux ratios that show marginal variations between 3.6 and 24 μm (see also Beaulieu et al. 2011). The interpretation of these broad-band spectrophotometry data is difficult and relies on statistical approaches (Madhusudhan & Seager 2011). Shabram et al. (2011) modelled the infrared transmission spectrum of GJ 436b. These authors conclude that the detailed infrared characterization of this planet may be possible using the *James Webb Space Telescope*. Before its launch, the use of UV facilities should be considered as a powerful way of characterizing the upper atmospheres of low-mass exoplanets.

6. Ly α emission of M dwarfs and stellar activity

Stellar Ly α emission lines are important spectral features in the context of exoplanet stellar environment and stellar physics. These emission lines are the main contributors to the flux of low-mass stars at short wavelengths, from X to FUV. For instance, the Ly α emission of the Sun contributes to more than 50% of its flux below 1216 Å (Woods et al. 1998). The Ly α line is used as a proxy for determining the temperature and pressure profiles of upper stellar atmospheres.

The Ly α emission originates in the transition regions between the chromospheres and coronae, while other commonly used activity diagnostics are based on indicators originating from the coronae (X-ray flux) or the chromospheres (Mg II *h* and *k* lines). In this context, stellar Ly α emission provides an almost unique access to the structure of the transition region, where the temperature profile exhibits a deep minimum. Houdebine & Doyle (1994) modelled the Ly α emission of M dwarfs. According to their work, the transition region of these stars is thinner than that of solar-like stars.

Stellar Ly α measurements are scarce in the literature. This is mainly because it is impossible to observe this emission from the ground and that it is difficult to correct measurements for the effects of the ISM absorption, both astrospheric and heliospheric absorption, and geocoronal emission. Furthermore, correlations between Ly α emission and other proxies of stellar activity can be misleading because they do not originate in the same region. This ensures that an accurate estimate of the Ly α brightness from an activity relation is rather hazardous. In addition, the Ly α line is extremely variable with time. For the Sun, the integrated Ly α line flux may change by 37% during one rotation and up to 50% over a couple of years (Vidal-Madjar 1975). During the magnetic cycle, the extreme (single day) values can vary by more than a factor of two (Woods et al. 2000).

Very few M dwarfs have Ly α measurements. Landsman & Simon (1993) used the *International Ultraviolet Explorer* (*IUE*) to report Ly α fluxes corrected from the ISM absorption for 12 M dwarfs. Wood et al. (2005) obtained resolved Ly α measurements for four M dwarfs with *HST/STIS*. Three objects are common to both samples, leading to a total of 13 measurements. This sample consists mostly of active stars. In particular, all the *HST* measurements of Wood et al. (2005) were obtained for M dwarfs with magnetic activity levels well above that of GJ 436. Therefore, our measurement of GJ 436's Ly α flux is invaluable

for estimating the properties of the transition region in quiet M dwarfs.

The measurements found in the literature are listed in Table 2. In Fig. 8, we have plotted the normalized Ly α flux, $R_{\text{Ly}\alpha} = f_{\text{Ly}\alpha}/f_{\text{bol}}$ as a function of the normalized X-ray flux $R_X = f_X/f_{\text{bol}}$ for the *IUE* and *HST* measurements from Table 2. We have not included the available data for YY Gemini and DT Virginis because these stars are close binaries for which a definitive identification of each component's flux is difficult. The values are listed in Table 2. The observed X-ray fluxes f_X are extracted from the *Rosat* all-sky survey (RASS) in the Nexxus 2 database (Schmitt & Liefke 2004). The bolometric fluxes f_{bol} are obtained by combining the *IK* photometry of Leggett (1992) with the bolometric correction BC_K versus $I - K$ relation of Leggett et al. (2000).

As can be seen in Fig. 8, the Ly α fluxes extracted from *HST* are significantly lower – for a given R_X – than those from *IUE*. Wood et al. (2005) note that the *HST* and *IUE* data are coherent for the majority of the objects (besides M dwarfs), except for the fainter ones for which the *IUE* fluxes are systematically higher than the *HST* ones. They attribute this to a bias in the corrections for the ISM absorption and geocoronal emission, which are particularly difficult at the lower resolution of *IUE*.

In the case of faint M dwarfs, we prefer to consider the clearly resolved *HST* measurements, which were obtained mainly for magnetically active stars. The values of $R_{\text{Ly}\alpha}$ seem to be correlated to R_X for M dwarfs, with $\log R_{\text{Ly}\alpha} \approx 0.5 \log R_X - 2.2$, although additional measurements are necessary to confirm this trend. The trend implies that $R_{\text{Ly}\alpha}/R_X > 1$ for quiet M dwarfs, in contrast to the results for more active ones. Figure 8 can thus be used – with caution – to estimate $R_{\text{Ly}\alpha}$ for all M dwarfs that have values of R_X between -5 and -3 , i.e., covering the domain of magnetic activity between 20% of that of the quietest M dwarfs in the solar neighbourhood to the very active stars close to the X-ray emission saturation level (see for instance Fig. 5 in Delfosse et al. 1998).

Meanwhile, we stress that the X-ray and Ly α fluxes have been measured here at different times and, therefore, for different magnetic states of the stars, which can add dispersion to any relationship. For GJ 436, the measured $\log L_X$ ranges from 25.96, as measured with *XMM-Newton* by Sanz-Forcada et al. (2010), to 27.15, as found in the *Rosat*/PSPC archives by Poppenhaeger et al. (2010). The value we have used throughout this work comes from the *Rosat* all-sky survey catalogue of the nearby stars (Hünsch et al. 1999) and is in-between these extreme values. The dispersion (standard deviation) in these three values is $\sigma_{L_X} = 0.77$.

We have retrieved all available X-ray measurements for the stars in Table 2 from the Nexxus 2 database and calculated their σ_{L_X} . However, these calculated dispersions only provide a rough idea of the real intrinsic X-ray variabilities of the listed M dwarfs, because the number of measurements (also reported in Table 2) is not equivalent for all stars. In addition, the measurements are derived using different instruments, mainly *Rosat* or *XMM-Newton* (or both). Differences between surveys, e.g. in the bandpasses, are not taken into account, thus adding to the dispersion. Finally, the occurrence of a flare during a given observation cannot be excluded, leading to a non-gaussian distribution of the measurements. Therefore, these values should only be regarded as indicative.

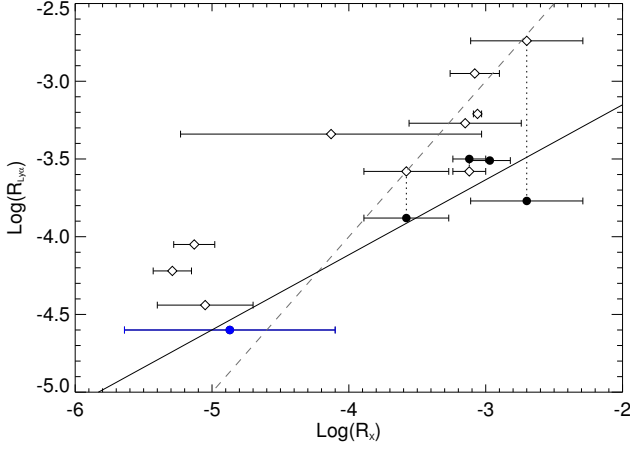


Fig. 8. Normalized Ly α flux $R_{Ly\alpha} = f_{Ly\alpha}/f_{bol}$ as a function of normalized X-ray flux $R_X = f_X/f_{bol}$ for all the *IUE* (\diamond) and *HST* (\bullet) Ly α flux measurements of M dwarfs in the literature. Our measurement for GJ 436 data is shown in blue. The dotted lines link *HST* and *IUE* measurements for objects that have been measured with both instruments. The plain line shows the best-fit linear regression to *HST* measurements, $\log(R_{Ly\alpha}) \approx 0.5 \log(R_X) - 2.2$. The grey dashed line indicates the $\log R_{Ly\alpha} = \log R_X$ relation. The horizontal error bars in the X-ray flux are the dispersions reported in Table 2.

Table 2. Normalized Ly α and X-ray fluxes of M dwarfs.

Star	Sp. T.	$R_{Ly\alpha}$	R_X^*	σ_{L_X} (dex)	N_X
Ly α from <i>HST</i>					
Proxima Cen	M6v	-3.88	-3.58	0.31 [†]	10
AD Leo	M4.5v	-3.50	-3.12	0.12 [†]	6
EV Lac	M3.5v	-3.77	-2.70	0.41 [†]	8
AU Mic	M1v	-3.51	-2.97	0.15 [†]	3
GJ 436	M2.5v	-4.60	-4.87	0.77 [§]	3
Ly α from <i>IUE</i>					
AX Mic	M0v	-4.22	-5.29	0.14 [†]	3
DT Vir	M2v	-3.27	-3.15	0.41 ^{†,‡}	5
GJ 887	M2v	-4.05	-5.13	0.15 [†]	2
GJ 411	M2v	-4.44	-5.05	0.35 [‡]	4
AD Leo	M4.5v	-3.58	-3.12	0.12 [†]	6
EV Lac	M3.5v	-2.74	-2.70	0.41 [†]	8
YZ CMi	M4.5v	-3.21	-3.06	0.03 ^{†,‡}	2
V1216 Sgr	M3v	-3.34	-4.13	1.10 ^{†,‡}	3
V998 Ori	M3.5v	-2.95	-3.08	0.18 [†]	2
Proxima Cen	M6v	-3.58	-3.58	0.31 [†]	10

Notes. (*) Normalized X luminosities are *Rosat* values extracted from the Nexxus 2 data base. The dispersion σ_{L_X} is the standard deviation in the N_X measurements found in the Nexxus 2 database. These measurements are derived using ([†]) *Rosat*, ([‡]) *XMM-Newton*, or (^{†,‡}) both. (§) The dispersion in the case of GJ 436 is obtained as the standard deviation in the three L_X values listed in the text.

7. Conclusion

We have obtained the first UV glance at a star hosting a transiting hot neptune. The *HST* data unambiguously show that the early and quiet M dwarf GJ 436 has bright Ly α emission. With an escape rate of around $\sim 10^{10}$ g s $^{-1}$, the hydrogen upper atmosphere of GJ 436b should cause large absorption ($\sim 11\%$) in

the Ly α transit light curve. These figures will allow the existence of such an extended upper atmosphere to be tested with a dedicated *HST* program. These results also suggest that other quiet M dwarfs are brighter at Ly α than in X-rays. This prediction opens new perspectives for the atmospheric characterization of other hot-neptune and even super-earth atmospheres. Interestingly, the nature of GJ 1214b, a super-earth, or ‘small-neptune’ also orbiting a quiet M dwarf (Charbonneau et al. 2009), could be resolved with this technique, provided the star is bright enough at Ly α .

Acknowledgements. We are particularly grateful to J.-M. Désert and A. Vidal-Madjar for their precious help with the preparation of the *HST* observations and comments on the manuscript. We thank the anonymous referee for a helpful review. We would also like to thank X. Bonfils, R. Ferlet, T. Forveille, G. Hébrard, A.-M. Lagrange, N. Meunier, and D. K. Sing for stimulating discussions. We also thank M. Mountain for awarding us *HST* DD time that made this work possible. D.E. is supported by the Centre National d’Études Spatiales (CNES).

References

- Ballester, G. E., Sing, D. K., Herbert, F. 2007, *Nature*, 445, 511
 Beaulieu, J.-P., Tinetti, G., Kipping, D. M., et al., *ApJ*, in press (arXiv:1007.0324)
 Butler, R. P. Vogt, S. S., Marcy, G. W., et al. 2004, *ApJ*, 617, 580
 Cecchi-Pestellini, C., Ciaravella, A., Micela, G., Penz, T. 2009, *A&A*, 496, 863
 Charbonneau, D., Brown, T. M., Latham, D. W., Mayor, M. 2000, *ApJ*, 529, L45
 Charbonneau, D., Brown, T. M., Noyes, R. W., Gilliland, R. L. 2002, *ApJ*, 568, 377
 Charbonneau, D., Berta, Z. K., Irwin, J., et al. 2009, *Nature*, 462, 891
 Davis, T. A., & Wheatley, P. J. 2009, *MNRAS*, 396, 1012
 Delfosse, X., Forveille, T., Perrier, C., Mayor, M. 1998, *A&A*, 331, 581
 Demory, B.-O., Gillon, M., Barman, T., et al. 2007, *A&A*, 475, 1125
 Dressel, L., et al. 2007, “STIS Data Handbook”, Version 5.0 (Baltimore: STScI)
 Ehrenreich, D. 2010, in *EAS Publication Series*, 41, Physics and Astrophysics of Planetary Systems, eds. T. Montmerle, D. Ehrenreich, A.-M. Lagrange, 429
 Ehrenreich, D., & Désert, J.-M. 2011, *A&A*, submitted
 Ehrenreich, D., Lecavelier des Etangs, A., Hébrard, G., et al. 2008, *A&A*, 483, 933
 Ferlet, R. D., André, M., Hébrard, G., et al. 2000, *ApJ*, 538, L69
 Figuera, P., Pont, F., Mordasini, C., et al. 2009, *A&A*, 493, 671
 Fossati, L., Haswell, C. A., Froning, C. S., et al. 2010, *ApJ*, 714, L222
 Fortney, J. J., Marley, M. S., Barnes, J. W. 2007, *ApJ*, 659, 1661
 García-Muñoz, A. 2007, *Planet. Space Sci.*, 55, 1426
 Gibson, N. P., Pont, F., Aigrain, S. 2010, *MNRAS*, in press (arXiv:1010.1753)
 Gillon, M., Pont, F., Demory, B.-O., et al. 2007a, *A&A*, 472, L13
 Gillon, M., Demory, B.-O., Barman, T., et al. 2007b, *A&A*, 471, L51
 Hébrard, G., & Moos, H. W. 2003, *ApJ*, 599, 297
 Henry, G. W., Marcy, G. W., Butler, R. P., Vogt, S. S. 2000, *ApJ*, 529, L41
 Houdebine, E. R., & Doyle, J. G., 1994, *A&A*, 289, 169
 Hüsch, M., Schmitt, J. H. M. M., Sterzik, M. F., Voges, W. 1999, *A&AS*, 135, 319
 Landsman, W., & Simon, T. 1993, *ApJ*, 408, 305
 Lecavelier des Etangs, A. 2007, *A&A*, 461, 1185
 Lecavelier des Etangs, A., Ehrenreich, D., Vidal-Madjar, A., et al. 2010, *A&A*, 514, A72
 Lecavelier des Etangs, A., Vidal-Madjar, A., Désert, J.-M. 2008, *Nature*, 456, E1
 Lecavelier des Etangs, A., Vidal-Madjar, A., McConnell, J. C., Hébrard, G. 2004, *A&A*, 418, L1
 Leggett, S. K. 1992, *ApJS*, 82, 351
 Leggett, S. K., Allard, F., Dahn C., et al. 2000, *ApJ*, 535, 965
 Linsky, J. L., Draine, B. T., Moos, H. W., et al. 2006, *ApJ*, 647, 1106
 Linsky, J. L., Yang, H., France, K., et al. 2010, *ApJ*, 717, 1291
 Madhusudhan, N., & Seager, S., submitted to *ApJ* (arXiv:1004.5121)
 Murray-Clay, R. A., Chiang, E. I., Murray, N. 2009, *ApJ*, 693, 23
 Perryman, M. A. C., Lindgren, L., Kovalevsky, J., et al. 1997, *A&A*, 323, L49
 Poppenhaeger, K., Robrade, J., Schmitt, J. H. M. M. 2010, *A&A*, 515, A98
 Pont, F., Gilliland, R. L., Knutson, H., Holman, M., Charbonneau, D. 2009, *MNRAS*, 393, L6
 Proffitt, C., et al. 2010, “STIS instrument handbook”, Version 9.0 (Baltimore: STScI)
 Sanz-Forcada, J., Ribas, I., Micela, G., et al. 2010, *A&A*, 511, L8
 Schmitt, J. H. M. M., & Liefke C. 2004, *A&A*, 417, 651
 Shabram, M., Fortney, J. J., Greene, T. P., Freedman, R. S. 2011, *ApJ*, 727, 65
 Stevenson, K. B., Harrington, J., Nymeyer, S., et al. 2010, *Nature*, 464, 1161
 Stone, J. M., & Proga, D. 2009, *ApJ*, 694, 205

- Torres, G. 2007, *ApJ*, 671, L65
- Tian, F., Toon, O. B., Pavlov, A. A., De Sterck, H. 2005, *ApJ*, 621, 1049
- Vidal-Madjar, A. 1975, *Sol. Phys.*, 40, 69
- Vidal-Madjar, A., Désert, J.-M., Lecavelier des Etangs, A., et al. 2004, *ApJ*, 604, L69
- Vidal-Madjar, A., Lecavelier des Etangs, A., Désert, J.-M., et al. 2003, *Nature*, 422, 143
- Vidal-Madjar, A., Sing, D. K., Lecavelier des Etangs, A., et al. 2011, *A&A*, in press (arXiv:1012.5938)
- Watson, A. J., Donahue, T. M., Walker, J. C. G. 1981, 48, 150
- Winn, J. 2010, *Transits and Occultations*. In *Exoplanets*, ed. S. Seager (Tucson: University of Arizona Press), in press
- Wood, B. E., Redfield, S., Linsky, J. L., Müller, H.-R., Zank, G. P. 2005, *ApJS*, 159, 118
- Woods, T. E., Eparvier, F. G., Bailey, S. M., et al. 2005, *J. Geophys. Res.*, 110, A01312
- Woods, T. E., Rottman, G. J., Bailey, S. M., Solomon, S. C. 1998, *Sol. Phys.*, 177, 133
- Woods, T. E., Tobiska, W. K., Rottman, G. J., Worden, J. R. 2000, *J. Geophys. Res.*, 105, 27195
- Woodgate, B. E., Kimble, R. A., Bowers, C. W., et al. 1997, *PASP*, 110, 1183
- Yelle, R. 2004, *Icarus*, 170, 167
- Yelle, R. 2006, *Icarus*, 183, 508